Pancreas and Cyst Segmentation

Konstantin Dmitriev, Ievgeniia Gutenko, Saad Nadeem, Arie Kaufman

Department of Computer Science, Stony Brook University, Stony Brook, NY 11794-2424 USA

ABSTRACT

Accurate segmentation of abdominal organs from medical images is an essential part of surgical planning and computer-aided disease diagnosis. Many existing algorithms are specialized for the segmentation of healthy organs. Cystic pancreas segmentation is especially challenging due to its low contrast boundaries, variability in shape, location and the stage of the pancreatic cancer. We present a semi-automatic segmentation algorithm for pancreata with cysts. In contrast to existing automatic segmentation approaches for healthy pancreas segmentation which are amenable to atlas/statistical shape approaches, a pancreas with cysts can have even higher variability with respect to the shape of the pancreas due to the size and shape of the cyst(s). Hence, fine results are better attained with semi-automatic steerable approaches. We use a novel combination of random walker and region growing approaches to delineate the boundaries of the pancreas and cysts with respective best Dice coefficients of 85.1% and 86.7%, and respective best volumetric overlap errors of 26.0% and 23.5%. Results show that the proposed algorithm for pancreas and pancreatic cyst segmentation is accurate and stable.

Keywords: Segmentation, Computed Tomography Images, Random Walker, Cyst, Pancreas.

1. INTRODUCTION

Being one of the deadliest of all the solid malignancies with a 7% five-year survival rate,[1] pancreatic cancer has become the third leading cause of cancer-related mortality in the United States. Normally, patients that have been diagnosed with pancreatic cancer have already reached a late stage. However, recent research has highlighted cysts as the precursors to pancreas cancer.[2] Hence, it is of the utmost importance to identify and remove malignant cysts in the early stages of pancreatic cancer to increase the survival chances of a patient. The increased use of high-resolution computed tomography and recent improvements in imaging technologies have significantly affected the accuracy of pancreatic imaging, and the potential for cyst identification and classification.

Segmentation of the pancreatic tissue and its masses is a crucial input to computer-aided diagnosis systems, which can help in surgery planning and navigation, as well as for automatic cancer detection and to provide an assessment of a disease. However, high interpatient variation in size, location (head, tail or body of the pancreas), and a lobulated shape of the organ pose a manual segmentation challenge even for an experienced radiologist. An area where the head of a pancreas connects to a duodenum is, in many cases, one of the hardest to segment. The most common challenges for segmentation of pancreatic mass segmentation are large variability in shape and location, as well as low contrasted boundaries (Figures 1 and 2).

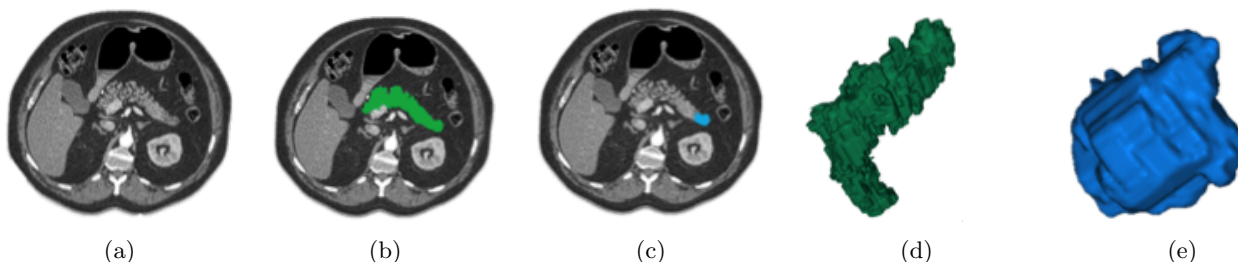(a)   (b)   (c)   (d)   (e)

Figure 1: Example of an Intraductal Papillary Mucinous Neoplasm (located in the tail of the pancreas): (a) initial axial slice, (b) the ground-truth pancreas segmentation, (c) the ground-truth cyst segmentation, (d) 3D view of the pancreas, (e) 3D view of the cyst.

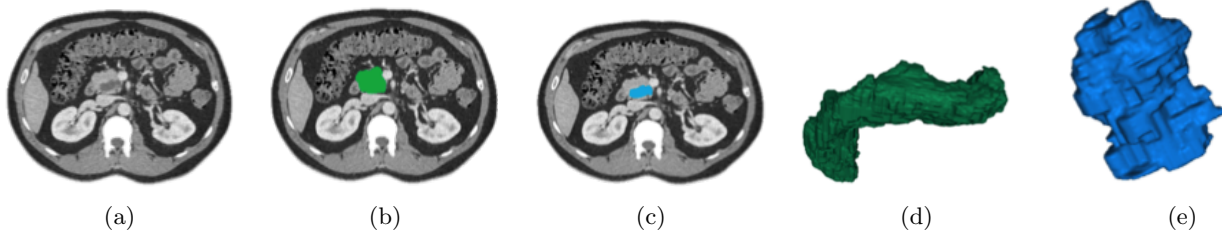(a)   (b)   (c)   (d)   (e)

Figure 2: Example of an Intraductal Papillary Mucinous Neoplasm (located in the head of the pancreas): (a) initial axial slice, (b) the ground-truth pancreas segmentation, (c) the ground-truth cyst segmentation, (d) 3D view of the pancreas, (e) 3D view of the cyst.

2. PREVIOUS WORK

Previous papers focus only on healthy pancreatic tissue segmentation. A great number of approaches rely on atlas based approaches and statistical shape modeling. Shimizu et al. have[3] proposed a pancreas segmentation algorithm which, at first, registers three-phase contrast-enhanced CT data for a particular patient and creates a probabilistic atlas guided segmentation, followed by a refinement stage with morphological operations and a classifier ensemble. Chu et al. have[4] performed multi-organ segmentation based on locally generated target-specific probabilistic atlases. Wolz et al have[5] combined a hierarchical atlas registration, weighting scheme, and graph-cuts. However, such shape-based methods often fail when the organ has abnormalities, since it is difficult to create a model which will cover all of the possible interpatient variabilities. Neural network based segmentation is another popular technique. State-of-the-art results for pancreas segmentation have been shown by Holger et al.[6] when utilizing a hierarchical coarse-to-fine classification of local image regions by deep convolutional networks. However, deep learning approaches are generally computationally expensive and there were no good results presented when applied for the segmentation of abnormal organs.

3. MATERIALS AND METHODS

This paper proposes a new semi-automatic approach for a pancreas segmentation, as well as pancreatic cystic masses, which is sensitive to inter-subject shape variability. Using a bounding box specified by a user and a few background/foreground seeds, we generate a rough segmentation, which is then refined by a random walker algorithm. The overall scheme of the proposed approach is illustrated in Figure 3.
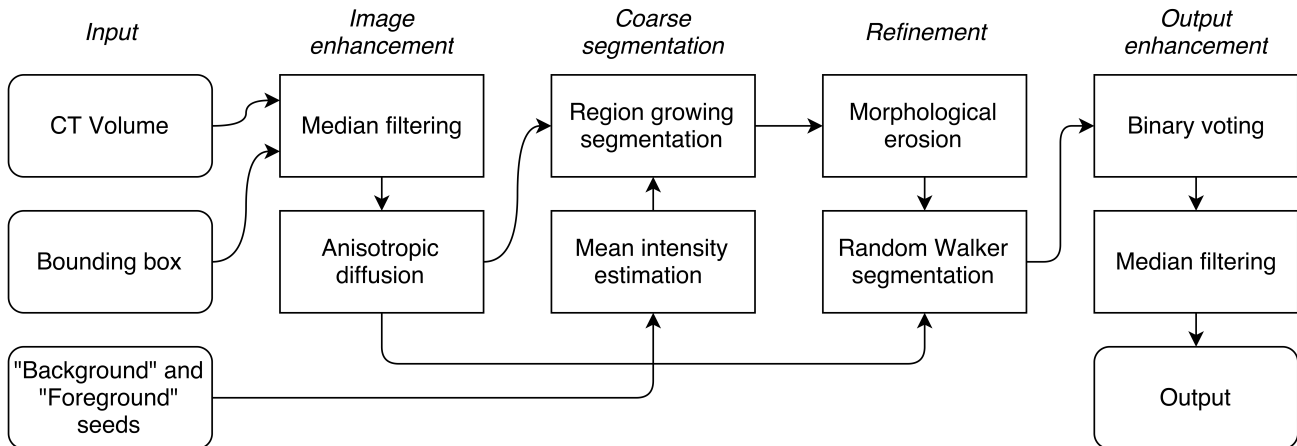

Figure 3: Overall segmentation scheme.

3.1 Subjects and data acquisition

The datasets consisted of 49 cases of abdominal CT scans presenting four different pancreatic neoplasms: Mucinous Cystic Neoplasm (MCN) – 11 cases, Serous Cystic Neoplasm (SCN) – 10 cases, Solid Pseudopapillary Neoplasm (SPN) – 8 cases, Intraductal Papillary Mucinous Neoplasm (IPMN) – 20 cases, which helped to develop (44 cases without manual segmentations) and test (5 cases with manual segmentations) the invariability of the algorithm with respect to varying pancreatic masses. All datasets followed the routine clinical protocols with portal venous phase of contrast enhancement and have an in-plane-resolution of 512x512 voxels with a slice thickness of 0.75mm.

3.2 Initialization via user interaction

The initial step is to refine a relatively large abdominal CT volume by parameterizing a particular region of interest (ROI) that contains the organ that needs to be segmented. For this purpose, the user selects two bounding points – the upper right and bottom left corners of the ROI, using axial, coronal, and/or sagittal views (Figure ??(a)). The user-specified bounding box helps not only to speed up the process of the segmentation by reducing the size of the initial volume, but also to ensure that the result of the segmentation will be within the the bounding box, which makes the proposed algorithm a highly reliable tool.

-

At the next step, a user puts a few seeds inside a selected ROI, highlighting voxels of the ROI that belong to an object to be segmented ("foreground") and all other voxels ("background"). The user can always readjust the seeds if they were placed incorrectly.

3.3 Image enhancement

Computed tomography images suffer from a high noise level. In order to reduce it, we apply a smoothing step (Figure ??(b)). We start with a median filter to remove impulsive noise. Since median filtering tends to remove fine details we decided to use a 3x3x3 box median filter, which yields good results in radiographic images without sacrificing the details.[7] We also include an additional edge preserving smoothing step that helps to improve the overall results. Most commonly used filters, such as the Gaussian filter, tend to affect object boundaries. We use anisotropic diffusion smoothing[8] that is controlled at the boundaries by a diffusion threshold, parameters for which are chosen after the empirical evaluation (conductance parameter – 0.5, gradient threshold – 15, number of iterations – 15). The resulting image provides sharper edges, while still reducing the noise.

3.4 Coarse segmentation

From the previously selected foreground seeds we estimate a mean intensity value μ of the object being segmented on the smoothed image. Using this value, we apply a region-growing algorithm (using 6-connected neighborhood), which selects voxels that can be classified as the foreground object based on an intensity range

$$[\mu - \sigma, \mu + \sigma], \tag{1}$$

where μ, σ are the mean and standard deviation of the intensities of the seed voxels, and rejects voxels that are connected to background seeds and the edges of the bounding box. The initial region growing begins from the user specified foreground seeds. The output of this step is a coarse segmentation of a foreground object (Figure ??(c)).

3.5 Refinement

A coarse segmentation from the previous step is refined by performing the random walker algorithm,[9] which allows us to obtain a high-quality segmentation. This algorithm uses a segmented image and a ternary image of markers (foreground, background and unlabeled), which is the output of the previous step. However, due to the poor contrast at the organ edges region-growing approaches might lend to leakages, Thus, in order to eliminate any possible leakage in foreground and background markers we perform morphological erosion (Figure ??(d, e)).

3.6 Output enhancement

Finally, we improve the result from the previous step by applying a binary voting scheme and a median filtering (3x3x3) for hole filling and smoothing, which helps to remove possible inaccuracies in the output from a previous step (Figure 4(f)).

4. RESULTS

The proposed algorithm was implemented as a combination of C++ and Python utilizing the Insight Toolkit Library[10] and SciPy Library.[11]

To evaluate the performance of the algorithm we compared the results of the segmentation with the respective manual ground-truth segmentations of the pancreas and cystic masses that were provided by an experienced radiologist. The pancreas and cyst segmentation were carried out in separate independent runs of the pipeline. To ensure the consistency of the results (which is an important problem in the manual segmentation as well[12]) we propose the following procedure: at first, the user has to perform the cyst segmentation, then the algorithm is allowed to use only unlabeled parts of the volume when performing the pancreas segmentation.

Analysis of the performance of the algorithm is done using the Dice similarity index (Eq. 2) and the volumetric overlap error (Eq. 3):

$$\frac{2|S \cap G|}{|S| + |G|}, \tag{2}$$

$$1 - \frac{|S \cap G|}{|S \cup G|}, \tag{3}$$

where S, G are output and manual segmentations, respectively.

The average results achieved by the proposed algorithm are presented in Table 1. The run time of the segmentation varies from 0.6 to 32.4 seconds (without manual interactions) per patient (8GB RAM, Intel Core i5-4308U 2.8Ghz). Figure 4 shows examples of worst, average, and best pancreas and pancreatic cyst segmentations. The best pancreas segmentation result (Figure 5(b)) (Dice 85.1%) is higher than the best segmentation from the state-of-the-art method[6] (Dice 80.0%). The cysts segmentation (Figure 5(d)) shows high results as well (Dice 86.7%). Figure 6 shows examples of the pancreas (green) and cyst (red) segmentation for different types of cysts.

Tissue	Volumetric Overlap Error (%)	Dice coefficient (%)
Healthy pancreas	43.5 ± 12.9	71.5 ± 10.5
Cyst	30.6 ± 12.8	81.4 ± 8.5

Table 1: Mean and standard deviation of the results of the segmentation for different types of tissue.
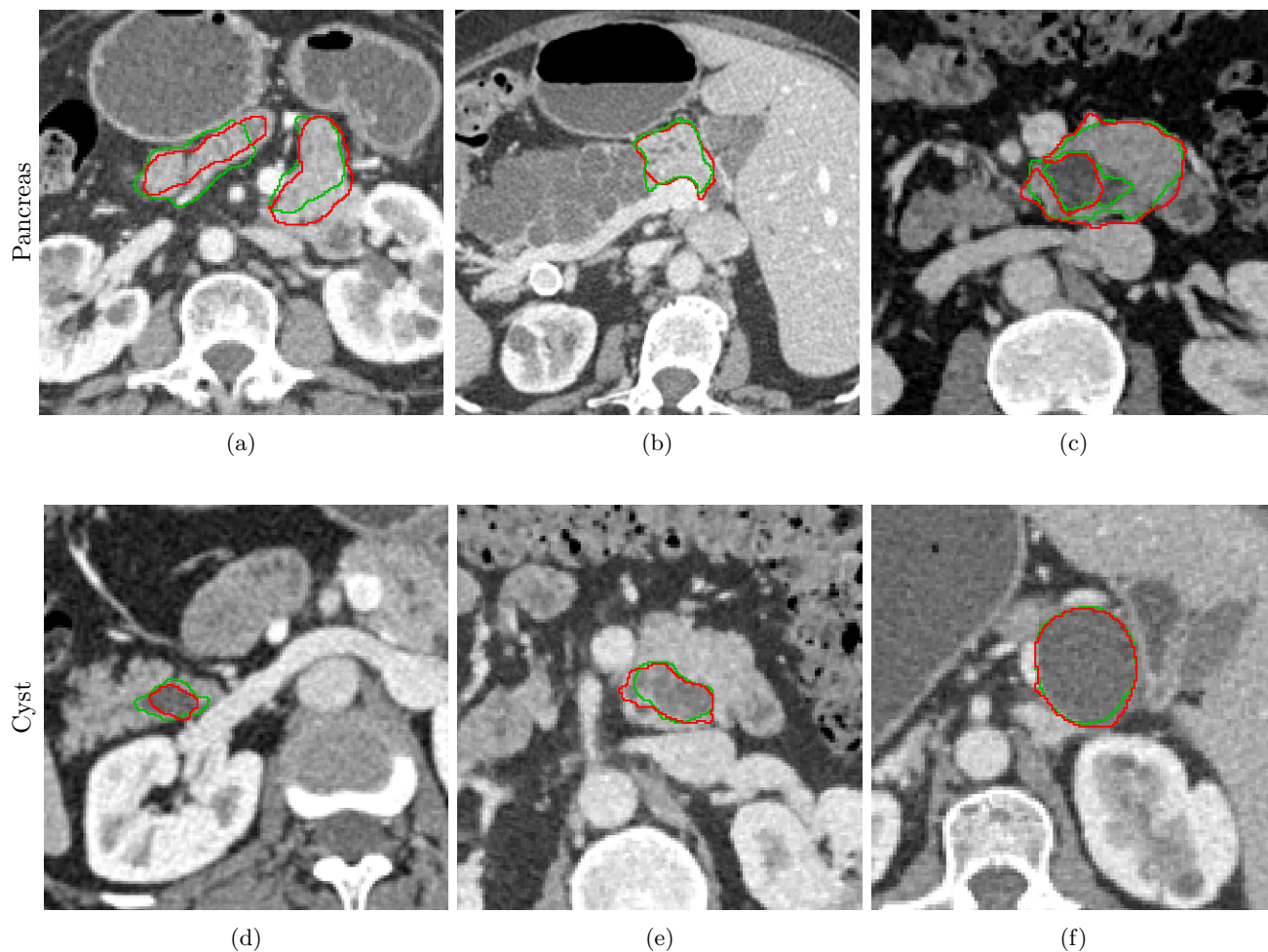
Figure 4: Examples of worst (a, d), average (b, e), and best (c, f) segmentation for the healthy pancreas tissue (top row) and cysts (bottom row). The manual segmentation is outlined in green, and the semi-automatic segmentation in red.
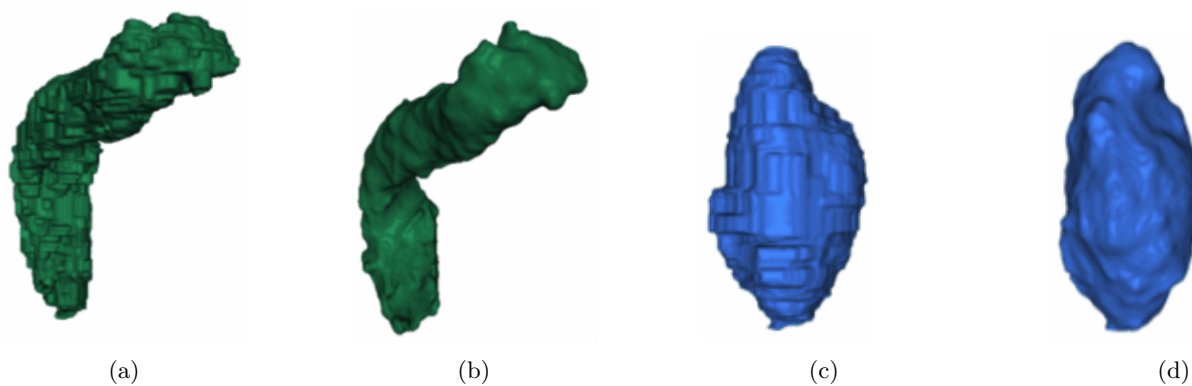

Figure 5: 3D visualization of the ground-truth (a, c) and examples of the results (b, d) of the pancreas (green) and of the cyst (blue).
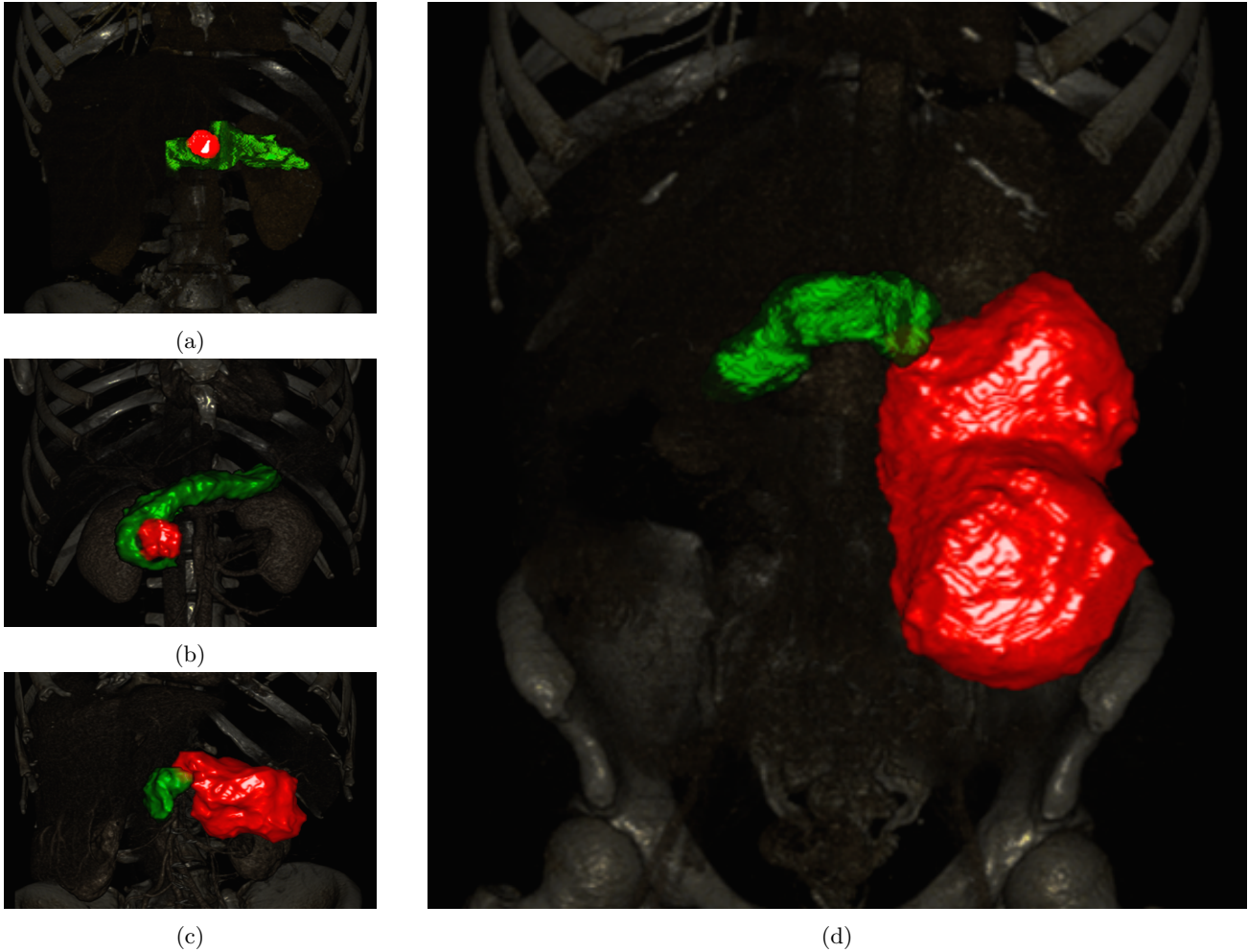
Figure 6: 3D visualization of the results for different types of cysts (green – pancreas; red – cyst). (a) Solid Pseudopapillary Neoplasm (SPN), (b) Intraductal Papillary Mucinous Neoplasm (IPMN), (c) Serous Cystic Neoplasm (SCN), (d) Mucinous Cystic Neoplasm (MCN).

5. CONCLUSION

This paper proposes a new semi-automatic technique for pancreas and pancreatic cyst segmentation. The effectiveness of this technique is demonstrated using abdominal CT datasets acquired during the venous phase. The strength of the presented method is a high precision segmentation achieved by the user-directed input. Although further verification studies are required, the described segmentation method shows promise for pancreas and pancreatic cyst segmentation.

ACKNOWLEDGEMENTS

REFERENCES

[1] Society, A. C., "American cancer society: Cancer facts and figures 2015," (2015).

[2] Hruban, R. H., Maitra, A., Kern, S. E., and Goggins, M., "Precursors to pancreatic cancer," *Gastroenterology Clinics of North America* **36**(4), 831–849 (2007).

[3] Shimizu, A., Kimoto, T., Kobatake, H., Nawano, S., and Shinozaki, K., "Automated pancreas segmentation from three-dimensional contrast-enhanced computed tomography," *International Journal of Computer Assisted Radiology and Surgery* **5**(1), 85–98 (2010).

[4] Chu, C., Oda, M., Kitasaka, T., Misawa, K., Fujiwara, M., Hayashi, Y., Nimura, Y., Rueckert, D., and Mori, K., "Multi-organ segmentation based on spatially-divided probabilistic atlas from 3D abdominal CT images," *Medical Image Computing and Computer-Assisted Intervention–MICCAI* , 165–172 (2013).

[5] Wolz, R., Chu, C., Misawa, K., Fujiwara, M., Mori, K., and Rueckert, D., "Automated abdominal multi-organ segmentation with subject-specific atlas generation," *IEEE Transactions on Medical Imaging* **32**(9), 1723–1730 (2013).

[6] Roth, H. R., Farag, A., Lu, L., Turkbey, E. B., and Summers, R. M., "Deep convolutional networks for pancreas segmentation in CT imaging," *Proc. of SPIE Medical Imaging* , 94131G–94131G (2015).

[7] Ritenour, E., Nelson, T., and Raff, U., "Applications of the median filter to digital radiographic images," *Proc. IEEE International Conference on Acoustics, Speech, and Signal Processing (ICASSP)* **9**, 251–254 (1984).

[8] Perona, P. and Malik, J., "Scale-space and edge detection using anisotropic diffusion," *IEEE Transactions on Pattern Analysis and Machine Intelligence* **12**(7), 629–639 (1990).

[9] Grady, L., "Random walks for image segmentation," *IEEE Transactions on Pattern Analysis and Machine Intelligence* **28**(11), 1768–1783 (2006).

[10] Johnson, H. J., McCormick, M., Ibáñez, L., and Consortium, T. I. S., *The ITK Software Guide*. Kitware, Inc., third ed. (2013).

[11] Jones, E., Oliphant, T., Peterson, P., et al., "SciPy: Open source scientific tools for Python." `http://www.scipy.org/` (2001–). [Online; accessed 2016-01-16].

[12] Ketting, C. H., Austin-Seymour, M., Kalet, I., Unger, J., Hummel, S., and Jacky, J., "Consistency of three-dimensional planning target volumes across physicians and institutions," *International Journal of Radiation Oncology Biology Physics* **37**(2), 445–453 (1997).